

Hybrid Beamforming Design for Wideband MmWave Full-Duplex Systems

Elyes Balti, *Student Member, IEEE*, and Brian L. Evans, *Fellow, IEEE*

Abstract—Full duplex (FD), which allows bidirectional transmission over the same resources, has the potential to reduce latency and double spectral efficiency. Recently, FD has been studied in 5G LTE millimeter wave cellular communications for New Radio in 3GPP releases 15–17. The primary drawback of FD is self-interference (SI). SI arises in the receiver for system 1 because it receives transmissions from itself and system 2. Because system 1 is much closer, SI can be several orders of magnitude greater than the received power from system 2, thereby severely degrading communication. In this paper, we design the spatial beamformers for the phase arrays that are already built into the FD relay to extend mmWave coverage to a single user. We propose to use alternating projections in designing the precoder and combiner to maximize the sum of the uplink and downlink spectral efficiency while bringing the SI below the noise floor. Our contributions include (1) all-digital and hybrid beamforming design algorithms for SI cancellation; and (2) communication performance analysis in terms of spectral efficiency, energy efficiency and outage probability. We compare the proposed algorithms against beam steering, singular value decomposition, and angle search techniques.

Index Terms—Full-Duplex, Self-Interference, Single-User MIMO, MmWave Cellular, Hybrid Beamforming

I. INTRODUCTION

For a couple of decades, wireless networks have been evolving to meet the exponential growth in demand for mobile data. In cellular networks, long-term evolution (LTE) standards have been increasing bandwidths, spectrum reuse, antennas, and modulation size accordingly since their launch in 2008. Fourth-generation (4G) LTE standards (2011–2018) use frequency bands below 6 GHz and can provide up to 100 MHz in effective bandwidth depending on the deployment. 5G LTE standards (2018–) not only continue using the 4G sub-6 GHz bands but also introduce millimeter wave (mmWave) frequency bands in the 10 to 300 GHz range¹. Designing beamforming (spatial filtering) algorithms for massive antenna arrays can overcome the high propagation losses in mmWave bands. 5G New Radio (NR) can achieve 10x increase in peak and average bit rates over 4G due to the large mmWave bandwidths, e.g. 700 MHz in the 24 GHz band and 850 MHz in the 28 GHz band. In 2012, prior to the 5G LTE standards, the Wi-Fi IEEE 802.11ad standard adopted usage of the unlicensed 57–64 GHz mmWave band to achieve high bit rates [1], [2].

Elyes Balti and Brian L. Evans are with the Wireless Networking and Communications Group, Department of Electrical and Computer Engineering, The University of Texas at Austin, Austin, TX 78712 USA (e-mails: ebalti@utexas.edu, bevans@ece.utexas.edu).

¹Although a rigorous definition of mmWave frequencies would place them between 30 and 300 GHz, industry has loosely defined them to include the spectrum from 10 to 300 GHz.

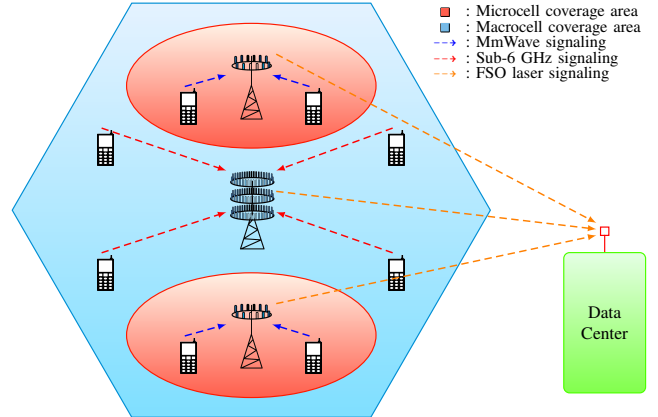


Fig. 1: Outdoor heterogeneous mmWave cellular relaying network with free space optics (FSO) backhauling wherein the base stations are playing the key role of relays to improve coverage. Sub-6 GHz communications take place within the macrocells (large area) where reliable links require high power to maintain coverage. In microcells, where cell area is small, mmWave signaling can reliably support high data rates to the users. [3]

Full duplex (FD) could potentially reduce latency and double spectral efficiency in mmWave communication systems. These improvements make FD mmWave transceivers a potential candidate for applications such as platooning, advanced driving assistance system, autonomous driving, and vehicular clouds, which require huge bandwidth, high data rate and low latency. Full duplex has been under study for New Radio by 3GPP Releases 15–17 for LTE standardization [4].

Fig. 1 illustrates an example FD cellular system. Because FD systems transmit and receive using the same resource blocks, FD transceivers are subject to the near-far problem. The near-far problem can be illustrated using point-to-point communications. In system 1, the receiver receives a signal from its transmitter that could be several orders of magnitude stronger than the transmitter in system 2 due to propagation losses over the longer distance. The near-far problem can result in severe communication degradation. In order to make FD systems practical, designing robust beamforming and interference cancellation techniques are critical.

A. Self-Interference Cancellation Techniques

1) *Antenna Array Architectures*: Interference cancellation can be realized by using antenna separation, isolation, polarization [5]–[8], directional antennas [9]–[11] or antenna placement to create null space at the receive arrays [12], [13]. The application of each technique depends solely on the hardware constraints and the application itself. For example, the application of passive SI cancellation using isolation and separation is limited for mobile devices due to their

small dimensions. Fortunately, interference suppression can be achieved in relaying systems because the transmit and receive arrays are not necessarily collocated. In addition, [7] showed that directional arrays with a range of 4–6m of antenna isolation can achieve a hefty amount of SI reduction as high as 80 dB. This extent of isolation can be applicable in relaying systems; however, mobile devices cannot support such isolation due to their relatively small dimensions.

2) *Analog Circuitry*: This approach aims to suppress the SI before the low noise amplifier (LNA) and analog-to-digital converter (ADC) by subtracting an estimate of the received SI from the received signal. The radio-frequency (RF) transmitted signal can be extracted at the transmit power amplifier (PA) output, processed in the RF SI cancellation stage and subtracted from the received signal. Analog RF SI-cancellation can be first applied [10], [11], [14] to suppress only the internal coupling and reflections modeled by a programmable analog tapped-delay line (TDL) transversal filter. Further adaptive digital RF cancellation can also be applied to suppress the SI components coming from the random external reflections by using a digital symbol-synchronous finite impulse-response (FIR) filter [9], [15], [16].

Traditionally, the analog RF cancellation uses the knowledge of the transmitted SI to cancel it before the receive LNA. A copy of the transmitted signal is obtained from the PA output and passed through a canceling circuit to reconstruct a copy of the received SI. The signal at the PA output includes the distortions of the transmitter (TX), which are reduced by the analog RF cancellation stage.

The canceling circuit design is related to the nature of the SI channel. The SI channel can be divided into internal reflections with a smaller number of paths, shorter delays and stronger amplitudes compared to the external (far-field) reflections. The static internal reflections are static as they depend on the internal components and structure of the transceiver, while the external reflections vary according to the surrounding environment. Since it is difficult to adapt the analog circuits with the variations of the external reflections, the analog RF cancellation stage reduces only the static internal reflections. A canceling circuit, such as a Renesas QHx220 chip, is used in [9], [16]. The chip takes the transmitted SI as input, changes its amplitude and phase to match the received SI, and subtracts the resulting signal from the received signal. This method achieves about 20 dB reduction in received SI [16].

3) *Digital Circuitry*: Processing the SI in the digital domain facilitates the use of adaptive filtering for a large number of reflected paths due to the external environment. The digital SI cancellation is based on the general transversal symbol-synchronous FIR structure where the constant tap-delay is equal to the signal sampling period and implemented as a D-flip flop clocked by the sampling clock. Here, only the tap-coefficients need to be specified from an estimate of the SI channel and thus we avoid the interaction between the delays and the attenuations as the case for the analog TDL. As a result, the digital processing can deal with a larger number of taps than the analog TDL to adapt to the varying external environment. The resulting canceling signal can be subtracted from the received signal at the RF input of the LNA/ADC to

further reduce the SI resulting from the external reflections and to keep the LNA/ADC from being overloaded. This operation requires an additional digital-to-analog (DAC) converter and an upconverting radio chain to generate the RF signal. The additional components will slightly change the generated SI leading to residual SI. This RF cancellation stage can provide 30 dB of SI cancellation [14], [15], which, on top of the previously obtained 45 dB, still leaves a large amount of SI.

The baseband cancellation stage represents the last line of defense against the SI by reducing it after the ADC. For this reason, we should estimate the TX nonlinearities and residual SI channel resulting from the difference between the actual SI channel and the equivalent channel generated by the previous cancellation stages. In addition, related work has proposed circuits for joint analog and digital SI cancellation. Digital SI cancellation is particularly suitable for MIMO systems as the cross-interference between antennas increases the number of taps needed to reduce the SI considerably. In the same context, an all-digital SI cancellation based on a new FD transceiver structure significantly reduces transceiver impairments [17]. This technique consists of an intermediary receiver (RX) chain to obtain a digital replica of the transmitted SI signal that will be used to cancel the SI signal and TX imperfections. The results show the combination of this digital technique and the passive RF cancellation significantly reduces the SI to be 3 dB higher than the noise floor, resulting in 67-76% rate enhancement compared to the conventional half duplex (HD) systems operating at 20dBm of transmit power [18].

4) *Spatial Beamforming*: Another technique, spatial suppression, has been effective in mitigating SI for FD MIMO system [19], [20]. This technique leverages available degrees of freedom (DoF) of the multiple antennas to cancel SI while maintaining an acceptable multiplexing gain. This approach does not require any additional analog circuitry. Analog beamforming architectures are cost-efficient because they only require phase shifters. However, such architecture is primarily constrained by the low quality and limited DoF of the phase shifters where the beam pattern is managed only through the phase shifters while keeping constant amplitudes (CA). The CA constraint introduces additional performance loss. Similar work [21] proposed a design to find the optimal analog beamformers; however, significant performance losses are introduced when projecting the solution onto the subspace of the CA constraint. This result was explained by the fact that the projection onto the CA subspace violates the interference cancellation constraint. In addition, related work proposed various hybrid beamforming designs for FD systems. For example, the work in [22] proposed an iterative optimization algorithm to minimize the SI power and improve the spectral efficiency while maintaining reasonable number of iterations for the convergence. Moreover, [23] proposed beamforming design algorithm to maximize the spectral efficiency for a dual-hop FD relaying system wherein the performances are compared to HD and upper bound as benchmarking.

B. Contributions

We consider a wideband mmWave cellular system in a single-user (SU) scenario where an FD base station (BS)

independently communicates with uplink and downlink user equipments (UEs). The goal is to design robust hybrid beamformers to cancel the loopback SI, avoid ADC saturation and provide the uplink UE with acceptable spectral efficiency relative to the downlink UE which is interference-free. The contributions follow:

- We aim for minimizing the SI power by jointly designing the full-digital beamformers for the base station and the UEs by using the *alternating projection* based on the idealized simplifying assumption of having perfect channel state information (CSI).
- We design in the second stage the analog beamformers by using *alternating projection* and then deriving closed-form solutions of the digital beamformers. With sufficient number of iterations, the hybrid beamforming algorithm mitigates the SI power and nearly approaches the interference-free downlink UE performance.
- We present quantitative comparisons of our proposed algorithms through simulation, wherein our proposed design achieves better performance gains than beam steering, Singular Value Decomposition (SVD) and angle search techniques.
- We analyze communication performance in terms of spectral efficiency, energy efficiency and outage probability. For spectral efficiency, we provide the full-digital beamformer and an upper bound to serve as benchmarking tools for the proposed hybrid beamformer.

C. Organization

The rest of the paper is organized as follows: Section 2 discusses the system and channel models, while the beamforming design for full-digital and hybrid architectures are detailed in Section 3. Energy efficiency and outage probability are analyzed in Section 4, whereas numerical results and their discussions appear in Section 5. Section 6 concludes the paper.

D. Notation

We use the following notation throughout the paper. We denote $(\cdot)^T$, $(\cdot)^*$, $(\cdot)^\dagger$ and $\mathbb{P}[\cdot]$ as the Transpose, Hermitian, Pseudo-Inverse and the probability measure operators, respectively. Moreover, $\|\cdot\|_F$ and $\det(\cdot)$ are the Frobenius norm and determinant, respectively. \mathbf{H} and \mathbf{H} are the discrete-time channel and its Fast Fourier Transform (FFT), respectively. In addition, \mathbf{I}_N is the identity matrix with size $N \times N$.

II. SYSTEM MODEL

Fig. 2 describes the wideband mmWave full-duplex system with hybrid analog/digital beamforming.

Wideband transmission uses OFDM signaling with K subcarriers. At the k -th subcarrier, the symbols $s[k]$ are transformed to the time domain using the K -point IDFT. The cyclic prefix (CP) of length (L_c) is then appended to the time domain samples before applying the precoder. The OFDM block is formed by the CP followed by the K time domain samples and the data symbols follows $\mathbb{E}[s[k]s^*[k]] = \frac{\rho}{KN_s}\mathbf{I}$, where ρ is the total average transmit power for the data

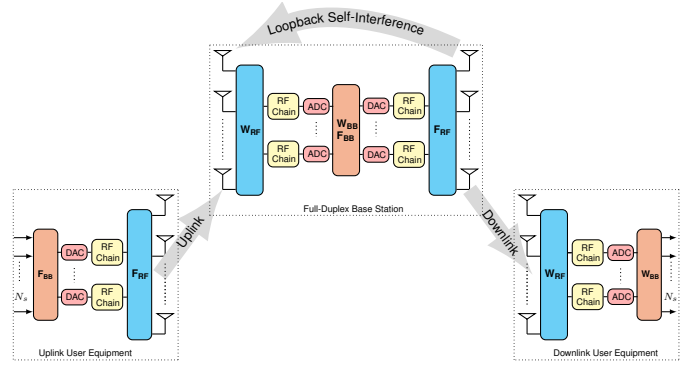


Fig. 2: Hybrid architecture of dual-hop FD relaying system. The uplink user equipment (UE) sends the data to the base station (BS) independently from the data intended to the downlink UE sent from the BS. Since the BS transmits and receives simultaneously at the same resource blocks, we model the SI leakage by the wideband channel matrix with the ℓ -th tap $\mathbf{H}_s[\ell]$.

i.e., without considering the CP, per OFDM symbol. We assume the maximum delay spread of the channel is within the CP duration. This description applies equally for uplink and downlink transmissions.

For uplink, the received signal at the BS in the k -th subcarrier is given by

$$y_{\text{uplink}}[k] = \sqrt{\rho_u} \mathbf{W}_{\text{BS}}^* [k] \mathbf{H}_u [k] \mathbf{F}_{\text{UE}} [k] \mathbf{s}_u [k] + \sqrt{\rho_s} \mathbf{W}_{\text{BS}}^* [k] \mathbf{H}_s [k] \mathbf{F}_{\text{BS}} [k] \mathbf{s}_d [k] + \mathbf{W}_{\text{BS}}^* [k] \mathbf{n}_{\text{BS}} [k] \quad (1)$$

where $\mathbf{W}_{\text{BS}} [k]$, $\mathbf{F}_{\text{BS}} [k]$, $\mathbf{F}_{\text{UE}} [k]$ being the k -th full-digital combiner, precoder at BS and k -th full-digital precoder at the uplink UE, respectively. $\mathbf{H}_u [k]$, $\mathbf{H}_s [k]$ being the k -th uplink and SI subcarriers, respectively, while $\mathbf{s}_u [k]$, $\mathbf{s}_d [k]$ and $\mathbf{n}_{\text{BS}} [k]$ being the UE data sent to BS, BS data sent to downlink UE and the additive white Gaussian noise (AWGN) at BS with zero-mean and variance σ_u^2 , respectively. Note that ρ_u and ρ_s are the average transmit power at BS and SI power, respectively.

For downlink scenario, the received signal at the UE and at the k -th subcarrier is expressed by

$$y_{\text{downlink}} [k] = \sqrt{\rho_d} \mathbf{W}_{\text{UE}}^* [k] \mathbf{H}_d [k] \mathbf{F}_{\text{BS}} [k] \mathbf{s}_d [k] + \mathbf{W}_{\text{UE}}^* [k] \mathbf{n}_{\text{UE}} [k] \quad (2)$$

where $\mathbf{W}_{\text{UE}} [k]$ is the k -th fully-digital combiner at the downlink UE, ρ_d is the UE received power from the BS, $\mathbf{n}_{\text{UE}} [k]$ is the AWGN at the UE with zero-mean and variance σ_d^2 and $\mathbf{H}_d [k]$ is the k -th downlink subcarrier. Unlike the downlink scenario, the uplink received signal is corrupted by the loopback SI at the FD BS.

A. Baseband Channel Model

In this work, we assume the uplink and downlink MIMO channels are wideband, with a delay tap length L in the time domain. The ℓ -th delay tap of the channel is represented by a $N_{\text{RX}} \times N_{\text{TX}}$ matrix, $\ell = 0, \dots, L-1$, which, assuming a geometric cluster and ray based channel model given by [24]

$$\mathbf{H}[\ell] = \sqrt{\frac{N_{\text{RX}} N_{\text{TX}}}{\gamma}} \sum_{c=0}^{C-1} \sum_{r_c=0}^{R_c-1} \alpha_{r_c} p(\ell T_s - \tau_c - \tau_{r_c}) \times \mathbf{a}_{\text{RX}}(\theta_c + \vartheta_{r_c}) \mathbf{a}_{\text{TX}}^*(\phi_c + \varphi_{r_c}) \quad (3)$$

where T_s is the signaling interval, τ_c is the mean time delay of the cluster, and θ_c and ϕ_c are the angles of arrival (AoA) and departure (AoD), respectively. Each ray has a relative time delay τ_{r_c} , relative AoA (ϑ_c) and AoD (φ_c) shifts, and a complex gain α_{r_c} . Here, γ is the pathloss and $p(\tau)$ is the raised cosine pulse shape evaluated at τ . In addition, $\mathbf{a}_{\text{RX}}(\theta)$ and $\mathbf{a}_{\text{TX}}(\phi)$ are the antenna array response vectors of the RX and TX, respectively. The RX array response vector is

$$\mathbf{a}_{\text{RX}}(\theta) = \frac{1}{\sqrt{N_{\text{RX}}}} \left[1, e^{j\frac{2\pi d}{\lambda} \sin(\theta)}, \dots, e^{j\frac{2\pi d}{\lambda} (N_{\text{RX}}-1) \sin(\theta)} \right]^T \quad (4)$$

The channel at the k -th subcarrier is given by

$$\mathbf{H}[k] = \sum_{\ell=0}^{L-1} \mathbf{H}[\ell] e^{-j\frac{2\pi k}{K} \ell} \quad (5)$$

where $k = 0, 1, \dots, K-1$.

B. Self-Interference Channel Model

As illustrated in Fig. 3, the SI leakage at the BS is modeled by the channel matrix \mathbf{H}_s . The SI channel is decomposed into line-of-sight (LOS) component modeled by \mathbf{H}_{los} and a non-line-of-sight (NLOS) leakage described by \mathbf{H}_{nlos} which follows the channel model (3). The LOS SI leakage matrix

$$[\mathbf{H}_{\text{los}}]_{pq} = \frac{1}{d_{pq}} e^{-j2\pi \frac{d_{pq}}{\lambda}} \quad (6)$$

where d_{pq} is the distance between the p -th antenna in the TX array and q -th antenna in the RX array at BS. The aggregate ℓ -th tap SI channel $\mathbf{H}_s[\ell]$ can be expressed as [25, Eq. (2)]

$$\mathbf{H}_s[\ell] = \underbrace{\sqrt{\frac{\kappa}{\kappa+1}} \mathbf{H}_{\text{los}}}_{\text{Near-Field}} + \underbrace{\sqrt{\frac{1}{\kappa+1}} \mathbf{H}_{\text{nlos}}[\ell]}_{\text{Far-Field}} \quad (7)$$

where κ is the Rician factor.

C. Transceiver Impairments

5G mmWave cellular systems operate in 24, 28, 37, 39 and 47 GHz bands. In US FCC auctions, the corresponding transmission bandwidths are 0.7, 0.85, 1, 1, and 1.4 GHz broken into 100 MHz subbands. MmWave systems need very large antenna arrays to overcome high propagation losses. The

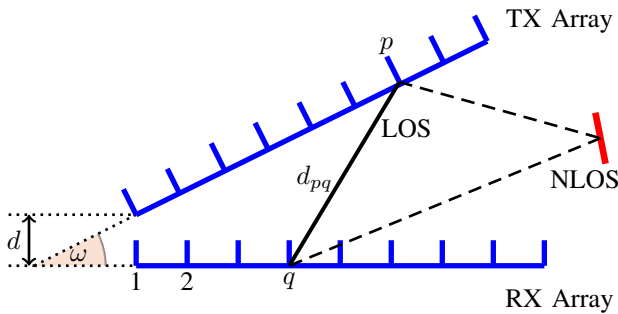


Fig. 3: Relative position of TX and RX arrays at the full-duplex BS. Since the TX and RX arrays are collocated, a far-field assumption that the SI signal impinges on the RX antenna array as a planar wave does not hold; instead, it is more suitable to assume the SI signal impinges as a spherical wave for the near-field LOS channel. [26]

massive jump in the number of antenna elements, transmission bandwidth, and data converter conversion rates for 5G mmWave systems has led to new basestation architectures for energy efficiency, such as hybrid analog/digital beamforming.

Introducing full-duplex transceivers also has several design challenges to achieve doubling spectral efficiency. High power amplifier (HPA) nonlinearity can severely degrade the system performance such as the creation of irreducible outage/error floor and/or spectral efficiency saturation. In addition, the amplifier produces intermodulation products that translate into spectral regrowth (or spectral shoulder) resulting in interference in adjacent subcarriers and loss of information.

Conventional techniques to compensate nonlinear effects include those based on Bussgang Linearization. Moreover, heuristic HPA nonlinearity models have been proposed such as soft envelope limiter, traveling wave tube amplifier, and solid state power amplifier [3], [27], [28].

Furthermore, mmWave transmitter impairments may affect SI cancellation for full-duplex systems. In order to subtract the received SI signal, any modifications that occur on the transmitter side have to be captured. This includes channel features and analog components such as the power amplifier and IQ mixer. The transmitted SI is slightly modified as it moves through the transmit chain and such modifications are relatively negligible compared to the desired signal; however, they are of significant magnitude compared to the intended signal and will limit the performance of full-duplex systems.

In practical implementations, the inband image resulting from the transmit IQ mixer is about 30 dB lower than the direct signal. In the presence of strong SI of about 50 dB higher than the transmit signal, this IQ image represents additional interference for the intended signal and also has to be reduced. Previous work selects transceiver component impairments for full-duplex transceivers [29]–[31]. Alternate high-speed DACs provide a direct conversion of the baseband signal to RF, also known as a direct RF transmitter. This technique can avoid many nonlinear distortions related to up-conversion.

The work in [32] consists of two full-duplex machine-to-machine nodes communicating over a bidirectional link. The direct and self-interference channels are narrowband. They propose full-digital and hybrid beamformers, and analyze spectral efficiency. In the next section, we modify the algorithms to support a full-duplex basestation communicating simultaneously with half-duplex uplink and downlink UEs; extend the framework to wideband uplink, downlink and self-interference MIMO channels; and investigate outage probability and energy efficiency in addition to spectral efficiency.

Remark. *Nonlinearities and other imperfections in mmWave analog/RF hardware have significant impact on full-duplex transceiver communication performance. Modeling transceiver hardware impairments is out of the scope of this work; however, we treat these impairments as additional sources of SI. For example, the aggregate SI power used in this work is around 120 dB. The near-far problem incurs an SI of about 20–60 dB (depending on whether the UE is near the BS, at mid-range or at the cell edge) and the remaining SI comes from transceiver impairments.*

III. BEAMFORMING DESIGN

A. Full-Digital Beamforming

In the full-digital domain, the uplink spectral efficiency is

$$\mathcal{I}(\rho_u) = \frac{1}{K} \sum_{k=0}^{K-1} \log \det (\mathbf{I}_{N_s} + \rho_u \mathbf{W}_{\text{BS}}^*[k] \mathbf{H}_u[k] \mathbf{F}_{\text{UE}}[k]) \quad (8)$$

$$\mathbf{Q}_u[k]^{-1} \mathbf{F}_{\text{UE}}^*[k] \mathbf{H}_u^*[k] \mathbf{W}_{\text{BS}}[k]$$

Here $\mathbf{Q}_u[k]$ is the SI plus noise covariance matrix at the k -th subcarrier given by

$$\mathbf{Q}_u[k] = \rho_s \mathbf{W}_{\text{BS}}^*[k] \mathbf{H}_s[k] \mathbf{F}_{\text{UE}}[k] \mathbf{F}_{\text{UE}}^*[k] \mathbf{H}_s^*[k] \mathbf{W}_{\text{BS}}[k] + \sigma_u^2 \mathbf{W}_{\text{BS}}^*[k] \mathbf{W}_{\text{BS}}[k]. \quad (9)$$

where $\sigma_u^2 = -173.8 \text{ dB} + 10 \log_{10}(\text{Bandwidth})$ [26].

For downlink scenario, the spectral efficiency is given by

$$\mathcal{I}(\rho_d) = \frac{1}{K} \sum_{k=0}^{K-1} \log \det (\mathbf{I}_{N_s} + \rho_d \mathbf{W}_{\text{UE}}^*[k] \mathbf{H}_d[k] \mathbf{F}_{\text{BS}}[k]) \quad (10)$$

$$\mathbf{Q}_d[k]^{-1} \mathbf{F}_{\text{BS}}^*[k] \mathbf{H}_d^*[k] \mathbf{W}_{\text{UE}}[k]$$

where $\mathbf{Q}_d[k]$ is the noise covariance matrix for the k -th subcarrier.

The objective of this design is to construct robust beamformers to provide the uplink UE with acceptable spectral efficiency compared to the downlink UE, given the former is affected by SI. We decompose the beamforming design into two phases. The first stage maximizes the rate for the uplink user, and the downlink user beamforming is designed in the second stage. Starting with the uplink scenario, we adopt a sub-optimal approach in which the zero-forcing constraint is imposed, thereby leading to the following optimization problem:

$$\max_{\mathbf{W}_{\text{BS}}[k], \mathbf{F}_{\text{BS}}[k], \mathbf{F}_{\text{UE}}[k], \mathbf{W}_{\text{UE}}[k]} \mathcal{I}(\rho_u) + \mathcal{I}(\rho_d) \quad (11)$$

$$k=0, \dots, K-1$$

Subject to $\mathbf{W}_{\text{BS}}^*[k] \mathbf{W}_{\text{BS}}[k] = \mathbf{I}_{N_s}$

$$\mathbf{F}_{\text{BS}}^*[k] \mathbf{F}_{\text{BS}}[k] = \mathbf{I}_{N_s}$$

$$\mathbf{F}_{\text{UE}}^*[k] \mathbf{F}_{\text{UE}}[k] = \mathbf{I}_{N_s}$$

$$\mathbf{W}_{\text{UE}}^*[k] \mathbf{W}_{\text{UE}}[k] = \mathbf{I}_{N_s}$$

$$\mathbf{W}_{\text{BS}}^*[k] \mathbf{H}_s[k] \mathbf{F}_{\text{BS}}[k] = \mathbf{0} \quad (\text{Zero-Forcing Constraint})$$

$$k = 0, \dots, K-1$$

We observe that the BS beamformers have to be jointly designed to maximize the beamformed received power and minimize the SI power simultaneously. In other terms, the BS beamformers are coupled in the uplink and downlink optimization. To cope with this problem, we fix the precoder and solve for the combiner and then fix the combiner and solve for the precoder, and this process will be repeated iteratively until the cost function is maximized. This process is also known as Zero-Forcing cyclic maximization and a convergence criterion should be triggered to stop the iterative process. The convergence is guaranteed since the cost function is bounded as the beamformers are normalized and the transmit power ρ is constrained. Accounting for the Zero-Forcing constraint, the optimization problem has the following generic form

$$\max_{\mathbf{X}} \log \det (\mathbf{I}_N + \rho \mathbf{X}^* \mathbf{A} \mathbf{A}^* \mathbf{X}) \quad (12)$$

Algorithm 1 Full-Digital Beamforming

```

1: function BASEBAND( $\mathbf{A}, \mathbf{C}, N$ )
2:    $\mathbf{P}_{\perp} \leftarrow \mathbf{I} - \mathbf{C}\mathbf{C}^{\dagger}$ 
3:    $\mathbf{X} \leftarrow N$  Dominant left singular vectors of  $\mathbf{P}_{\perp} \mathbf{A}$ 
4:   return  $\mathbf{X}$ 
5: end function

6: Input  $\mathbf{H}_s[k], \mathbf{H}_u[k], \mathbf{H}_d[k], k = 0, \dots, K-1$ 
7: Initialize  $\mathbf{F}_{\text{BS}}[k], \mathbf{F}_{\text{UE}}[k], k = 0, \dots, K-1$ 
8: for  $k \leftarrow 0 : K-1$  do
9:   for  $t \leftarrow 1 : N_{\text{outer}}$  do
10:     $\mathbf{W}_{\text{BS}}[k] \leftarrow$  BASE-
    BAND( $\mathbf{H}_u[k] \mathbf{F}_{\text{UE}}[k], \mathbf{H}_s[k] \mathbf{F}_{\text{BS}}[k], N_s$ )
11:     $\mathbf{F}_{\text{UE}}[k] \leftarrow N_s$  Dominant left singular vectors of
     $\mathbf{H}_u^*[k] \mathbf{W}_{\text{BS}}[k]$ 
12:     $\mathbf{W}_{\text{UE}}[k] \leftarrow N_s$  Dominant left singular vectors of
     $\mathbf{H}_d[k] \mathbf{F}_{\text{BS}}[k]$ 
13:     $\mathbf{F}_{\text{BS}}[k] \leftarrow$  BASE-
    BAND( $\mathbf{H}_d^*[k] \mathbf{W}_{\text{UE}}[k], \mathbf{H}_s^*[k] \mathbf{W}_{\text{BS}}[k], N_s$ )
14:   end for
15: end for
16: return  $\mathbf{F}_{\text{BS}}[k], \mathbf{W}_{\text{BS}}[k], \mathbf{W}_{\text{UE}}[k], \mathbf{F}_{\text{UE}}[k], k = 0, \dots, K-1$ 

```

$$\text{Subject to } \mathbf{X}^* \mathbf{X} = \mathbf{I}_N$$

$$\mathbf{X}^* \mathbf{C} = \mathbf{0}$$

where $\mathbf{X} \in \mathbb{C}^{M \times N}$ is the beamformer variable, $\mathbf{A} \in \mathbb{C}^{M \times N}$ is a given beamformed subcarrier and $\mathbf{C} \in \mathbb{C}^{M \times P}$ is a given beamformed SI channel that spans the SI subspace. Note that this generic form is to design the beamformer for a single subcarrier. Thereby, this routine will be repeated for all the system subcarriers. The solution to this problem is summarized by Algorithm 1. Note that the proof to the solution is given by [32, Appendix A].

Remark. Given the solution matrix $\mathbf{X} \in \mathbb{C}^{M \times N}$, which is the digital beamformer solution to the problem, M and N are the numbers of antennas and spatial streams, respectively. M should be large enough to sustain N spatial streams and the remaining $P = M - N$ degrees of freedom should be used to cancel the SI.

B. Hybrid Beamforming

In this part, we decompose the full-digital beamformers into their equivalent analog and digital factors. The analog beamformers are restricted by the constant amplitude (CA) hardware constraint. This constraint restricts the control of the array beam by tuning the phase shifters while keeping the amplitudes constant. The CA constraint defines the set of feasible solutions or equivalently the CA subspace. Like the full-digital beamforming design, we adopt the same Zero-Forcing cyclic maximization process. Starting with the formulation of the optimization problem as follows:

$$\max_{\mathbf{W}_{\text{BS,RF}}[k], \mathbf{F}_{\text{BS,RF}}[k], \mathbf{F}_{\text{UE,RF}}[k], \mathbf{W}_{\text{UE,RF}}[k], \mathbf{W}_{\text{BS,BB}}[k], \mathbf{F}_{\text{BS,BB}}[k], \mathbf{F}_{\text{UE,BB}}[k], \mathbf{W}_{\text{UE,BB}}[k]} \mathcal{I}(\rho_u) + \mathcal{I}(\rho_d) \quad (13)$$

$$k=0, \dots, K-1$$

$$\begin{aligned}
\text{Subject to } \mathbf{W}_{\text{BS}}[k] &= \mathbf{W}_{\text{BS,RF}} \mathbf{W}_{\text{BS,BB}}[k] \\
\mathbf{W}_{\text{BS}}^*[k] \mathbf{W}_{\text{BS}}[k] &= \mathbf{I}_{N_s} \\
\mathbf{F}_{\text{BS}}[k] &= \mathbf{F}_{\text{BS,RF}} \mathbf{F}_{\text{BS,BB}}[k] \\
\mathbf{F}_{\text{BS}}^*[k] \mathbf{F}_{\text{BS}}[k] &= \mathbf{I}_{N_s} \\
\mathbf{F}_{\text{UE}}[k] &= \mathbf{F}_{\text{UE,RF}} \mathbf{F}_{\text{BS,BB}}[k] \\
\mathbf{F}_{\text{UE}}^*[k] \mathbf{F}_{\text{UE}}[k] &= \mathbf{I}_{N_s} \\
\mathbf{W}_{\text{UE}}[k] &= \mathbf{W}_{\text{UE,RF}} \mathbf{W}_{\text{UE,BB}}[k] \\
\mathbf{W}_{\text{UE}}^*[k] \mathbf{W}_{\text{UE}}[k] &= \mathbf{I}_{N_s} \\
\mathbf{W}_{\text{BS,RF}}^* \mathbf{G}_s \mathbf{F}_{\text{BS,RF}} &= \mathbf{0} \\
\mathbf{W}_{\text{BS,RF}}, \mathbf{F}_{\text{BS,RF}} &\in \mathbb{V}^{N_{\text{BS}} \times N_{\text{RF}}} \\
\mathbf{W}_{\text{UE,RF}}, \mathbf{F}_{\text{UE,RF}} &\in \mathbb{V}^{N_{\text{UE}} \times N_{\text{RF}}} \\
k &= 0, \dots, K-1
\end{aligned}$$

where \mathbf{G}_s is the SI subcarrier with the lowest energy, $\mathbb{V}^{M \times L}$ is the set of feasible analog solutions or the CA subspace. Note that the Zero-Forcing constraint is defined in the analog and not in the digital domain in order to cancel the SI before the downconversion, sampling and quantization and hence avoiding the ADC saturation by the high SI levels. Like the full-digital case, the optimization problem for hybrid beamforming has the following generic form

$$\max_{\mathbf{X}_{\text{BB}}, \mathbf{X}_{\text{RF}}} \log \det (\mathbf{I}_N + \rho \mathbf{X}_{\text{BB}}^* \mathbf{X}_{\text{RF}}^* \mathbf{A} \mathbf{A}^* \mathbf{X}_{\text{RF}} \mathbf{X}_{\text{BB}}) \quad (14)$$

$$\begin{aligned}
\text{Subject to } \mathbf{X}_{\text{BB}}^* \mathbf{X}_{\text{RF}}^* \mathbf{X}_{\text{RF}} \mathbf{X}_{\text{BB}} &= \mathbf{I}_N \\
\mathbf{X}_{\text{RF}}^* \mathbf{C} &= \mathbf{0} \\
\mathbf{X}_{\text{RF}} &\in \mathbb{V}^{M \times L}
\end{aligned}$$

Note that $\mathbf{X}_{\text{RF}} \in \mathbb{C}^{M \times L}$ and $\mathbf{X}_{\text{BB}} \in \mathbb{C}^{L \times N}$ are the optimization variables, $\mathbf{A} \in \mathbb{C}^{M \times N}$, $\mathbf{C} \in \mathbb{C}^{M \times P}$ are given matrices. The constraints show that the analog beamformer should satisfy both the Zero-Forcing and CA constraints. In fact, imperfect SI cancellation may introduce severe degradation into the spectral efficiency and this might occur because the analog beamformers need not only to be projected onto the SI null subspace but also projected onto the CA subspace. The projection onto the latter subspace may violate the Zero-Forcing constraint and hence the SI may not be perfectly eliminated. For example, the authors in [33] discussed how the CA constraint ($\mathbf{X}_{\text{RF}} \in \mathbb{V}^{M \times L}$) violated the Zero-Forcing condition ($\mathbf{X}_{\text{RF}}^* \mathbf{C} = \mathbf{0}$) and they quantified the losses in terms of spectral efficiency. To circumvent this limitation, a common approach to solve such problem is to use the *Alternating Projection* method [34] which has been shown to yield better results for analog-only architecture [35].

In this work, we alternately project the analog beamformers between CA and Zero-Forcing subspaces to find a common subspace that optimally satisfies both conditions. The convergence after successive iterations of alternating projection provides the optimal subspace that eliminates SI and maximizes the sum spectral efficiency. To satisfy both conditions, we propose a two nested iterative loops wherein the outer loop handles the Zero-Forcing cyclic maximization (like full-digital case) while the inner loop deals with the alternating projection. Because closed-form analog solutions do not exist for (14), the optimal digital solution \mathbf{X}_{BB} can be expressed in terms of the

analog beamformers. The proof of the optimal digital solution is provided in [32, Appendix B]. More detailed analysis of the hybrid beamforming design is reported in Algorithm 2.

Algorithm 2 Hybrid Beamforming

```

1: function ANALOG( $\mathbf{A}, \mathbf{C}, L$ )
2:    $\mathbf{X}_{\text{RF}} \leftarrow L$  Dominant left singular vectors of  $\mathbf{A}$ 
3:    $\mathbf{P}_{\perp} \leftarrow \mathbf{I} - \mathbf{C}\mathbf{C}^{\dagger}$ 
4:   for  $k \leftarrow 1 : N_{\text{inner}}$  do
5:      $\mathbf{Y} \leftarrow \mathbf{P}_{\perp} \mathbf{X}_{\text{RF}}$ 
6:     for  $i \leftarrow 1 : M$  and  $j \leftarrow 1 : L$  do
7:        $(\mathbf{X}_{\text{RF}})_{ij} \leftarrow \frac{(\mathbf{Y})_{ij}}{|\mathbf{Y}_{ij}|}$ 
8:     end for
9:   end for
10:  return  $\mathbf{X}_{\text{RF}}$ 
11: end function

12: function DIGITAL( $\mathbf{X}_{\text{RF}}, \mathbf{A}, N$ )
13:  Compute SVD  $\mathbf{X}_{\text{RF}} = \mathbf{U}_{\text{RF}} \mathbf{S}_{\text{RF}} \mathbf{V}_{\text{RF}}^*$ 
14:   $\mathbf{Q} \leftarrow N$  Dominant left singular vectors of  $\mathbf{U}_{\text{RF}}^* \mathbf{A}$ 
15:   $\mathbf{X}_{\text{BB}} \leftarrow \mathbf{V}_{\text{RF}} \mathbf{S}_{\text{RF}}^{-1} \mathbf{Q}$ 
16:  return  $\mathbf{X}_{\text{BB}}$ 
17: end function

18: Input  $\mathbf{H}_s[k], \mathbf{H}_u[k], \mathbf{H}_d[k]$ ,  $k = 0, \dots, K-1$ 
19: Select uplink/downlink subcarrier of highest energy
20:  $k^* = \max_{k=0, \dots, K-1} \|\mathbf{H}[k]\|_F^2$ 
21: Select SI subcarrier of lowest energy
22:  $k^* = \min_{k=0, \dots, K-1} \|\mathbf{H}_s[k]\|_F^2$ 
23: Set  $\mathbf{G}_u \leftarrow \mathbf{H}_u[k^*]$ ,  $\mathbf{G}_d \leftarrow \mathbf{H}_d[k^*]$  and  $\mathbf{G}_s \leftarrow \mathbf{H}_s[k^*]$ 
24: Initialize  $\mathbf{F}_{\text{RF,BS}}, \mathbf{F}_{\text{RF,UE}}, \mathbf{F}_{\text{BB,BS}}[k], \mathbf{F}_{\text{BB,UE}}[k]$ ,  $k = 0, \dots, K-1$ 
25: Set  $\mathbf{F}_{\text{UE}}[k] \leftarrow \mathbf{F}_{\text{RF,UE}} \mathbf{F}_{\text{BB,UE}}[k]$ ,  $k = 0, \dots, K-1$ 
26: Set  $\mathbf{F}_{\text{BS}}[k] \leftarrow \mathbf{F}_{\text{RF,BS}} \mathbf{F}_{\text{BB,BS}}[k]$ ,  $k = 0, \dots, K-1$ 
27: for  $k \leftarrow 0 : K-1$  do
28:   for  $t \leftarrow 1 : N_{\text{outer}}$  do
29:      $\mathbf{W}_{\text{RF,BS}} \leftarrow \text{ANALOG}(\mathbf{G}_u \mathbf{F}_{\text{UE}}[k^*], \mathbf{G}_s \mathbf{F}_{\text{RF,BS}}, N_{\text{RF}})$ 
30:      $\mathbf{W}_{\text{BB,BS}}[k] \leftarrow \text{DIGITAL}(\mathbf{W}_{\text{RF,BS}}, \mathbf{H}_u[k] \mathbf{F}_{\text{UE}}[k], N_s)$ 
31:     Set  $\mathbf{W}_{\text{BS}}[k] \leftarrow \mathbf{W}_{\text{RF,BS}} \mathbf{W}_{\text{BB,BS}}[k]$ 
32:      $\mathbf{W}_{\text{RF,UE}} \leftarrow N_{\text{RF}}$  Dominant left singular vectors of  $\mathbf{G}_d \mathbf{F}_{\text{BS}}[k^*]$ 
33:      $\mathbf{W}_{\text{BB,UE}}[k] \leftarrow \text{DIGITAL}(\mathbf{W}_{\text{RF,UE}}, \mathbf{H}_d[k] \mathbf{F}_{\text{BS}}[k], N_s)$ 
34:     Set  $\mathbf{W}_{\text{UE}}[k] \leftarrow \mathbf{W}_{\text{RF,UE}} \mathbf{W}_{\text{BB,UE}}[k]$ 
35:      $\mathbf{F}_{\text{RF,UE}} \leftarrow N_{\text{RF}}$  Dominant left singular vectors of  $\mathbf{G}_u^* \mathbf{W}_{\text{BS}}[k^*]$ 
36:      $\mathbf{F}_{\text{BB,UE}}[k] \leftarrow \text{DIGITAL}(\mathbf{F}_{\text{RF,UE}}, \mathbf{H}_u^*[k] \mathbf{W}_{\text{BS}}[k], N_s)$ 
37:     Set  $\mathbf{F}_{\text{UE}}[k] \leftarrow \mathbf{F}_{\text{RF,UE}} \mathbf{F}_{\text{BB,UE}}[k]$ 
38:      $\mathbf{F}_{\text{RF,BS}} \leftarrow \text{ANALOG}(\mathbf{G}_d^* \mathbf{W}_{\text{UE}}[k^*], \mathbf{G}_s^* \mathbf{W}_{\text{RF,BS}}, N_{\text{RF}})$ 
39:      $\mathbf{F}_{\text{BB,BS}}[k] \leftarrow \text{DIGITAL}(\mathbf{F}_{\text{RF,BS}}, \mathbf{H}_d^*[k] \mathbf{W}_{\text{UE}}[k], N_s)$ 
40:     Set  $\mathbf{F}_{\text{BS}}[k] \leftarrow \mathbf{F}_{\text{RF,BS}} \mathbf{F}_{\text{BB,BS}}[k]$ 
41:   end for
42: end for
43: return  $\mathbf{F}_{\text{BS}}[k], \mathbf{W}_{\text{BS}}[k], \mathbf{W}_{\text{UE}}[k], \mathbf{F}_{\text{UE}}[k]$ ,  $k = 0, \dots, K-1$ 

```

IV. PERFORMANCE ANALYSIS

A. Energy Efficiency

The energy efficiency, expressed in bits/s/Hz/Watt or bits/J/Hz, is defined as the ratio between the spectral efficiency

and the total power consumption. It is expressed as

$$\mathcal{J}(\rho) = \frac{\mathcal{I}(\rho)}{\rho_{\text{Total}}} \quad (15)$$

where ρ_{Total} is the total power consumption. We adopt full-digital and hybrid combiners (DC and HC) where the total power consumption model for each architecture is defined by

$$\rho_{\text{Total}}^{\text{DC}} = N_{\text{RX}} (\rho_{\text{LNA}} + \rho_{\text{RF}} + 2\rho_{\text{ADC}}) \quad (16)$$

$$\rho_{\text{Total}}^{\text{HC}} = N_{\text{RX}} (\rho_{\text{LNA}} + \rho_{\text{SP}} + N_{\text{RF}}\rho_{\text{PS}}) + N_{\text{RF}} (\rho_{\text{RF}} + \rho_{\text{C}} + 2\rho_{\text{ADC}}) \quad (17)$$

where ρ_{RF} is the power consumption per RF chain which is defined by

$$\rho_{\text{RF}} = \rho_{\text{M}} + \rho_{\text{LO}} + \rho_{\text{LPF}} + \rho_{\text{BB}_{\text{amp}}} \quad (18)$$

TABLE I
POWER CONSUMPTION OF EACH DEVICE [36].

Device	Notation	Value
Low Noise Amplifier (LNA) [37]	ρ_{LNA}	39 mW
Splitter	ρ_{SP}	19.5 mW
Combiner [37]	ρ_{C}	19.5 mW
Phase Shifter [38], [39]	ρ_{PS}	2 mW
Mixer [40]	ρ_{M}	16.8 mW
Local Oscillator [41]	ρ_{LO}	5 mW
Low Pass Filter [41]	ρ_{LPF}	14 mW
Baseband Amplifier [41]	$\rho_{\text{BB}_{\text{amp}}}$	5 mW
ADC	ρ_{ADC}	Table III

B. Outage Probability

Once a transmission strategy is specified, the corresponding outage probability for rate R (bits/s/Hz) is then

$$P_{\text{out}}(\text{SNR}, R) = \mathbb{P}[\mathcal{I}(\text{SNR}) < R]. \quad (19)$$

With powerful channel codes, the probability of error when there is no outage is very small and hence the outage probability is an accurate approximation for the actual block error probability. Modern radio systems such as UMTS and LTE operate at a target error probability. Therefore, the primary performance measure is the maximum rate² at each SNR, such that the outage probability is less than ϵ , i.e.,

$$R_{\epsilon}(\text{SNR}) = \max_{\zeta} \{\zeta : P_{\text{out}}(\text{SNR}, \zeta) \leq \epsilon\} \quad (20)$$

C. Upper Bound

For interference-free scenario, the optimal beamformers diagonalize the channel. By applying the SVD successively on all subcarriers, we retrieve the singular values associated to each subcarrier matrix. For each subcarrier, the singular values are listed in descending order and we will extract the

²In this work, we define the notion of rate with outage as the average data rate that is correctly received/decoded at the receiver which is equivalent to the throughput. In other standards in the literature, the rate with outage is assimilated with the transmit data rate. The only difference is if we consider rate with outage as the throughput, we account for the probability of bursts (outage) and we multiply by the term $(1-\epsilon)$, while for the transmit data rate, the term $(1-\epsilon)$ is not accounted anymore.

first N_s modes associated to the spatial streams. Equivalently, the upper bound is given by

$$\mathcal{I}(\text{SNR}) = \frac{1}{K} \sum_{k=0}^{K-1} \sum_{\ell=0}^{N_s-1} \log \left(1 + \frac{\text{SNR}}{KN_s} \sigma_{\ell}(\mathbf{H}[k])^2 \right) \quad (21)$$

where $\sigma_{\ell}(\mathbf{H})$ is the ℓ -th singular value of the channel matrix \mathbf{H} . Note that the upper bound derivation follows the same rules for uplink as well as the downlink scenario.

V. NUMERICAL RESULTS

In this section, we discuss the numerical results of the communication performance measures obtained by Monte Carlo simulation³. Unless otherwise stated, Table II illustrates the values of the system parameters.

TABLE II
SYSTEM PARAMETERS [24].

Parameter	mmWave	Sub-6 GHz
Carrier frequency	28 GHz	3.5 GHz
Bandwidth	850 MHz	150 MHz
Number UE antennas	4	2
Number relay/BS antennas	16TX+16 RX	8TX+8RX
Antenna separation	$\lambda/2$	$\lambda/2$
Antenna correlation	None	None
Number clusters	4	10
Number rays per cluster	10	20
Angular spread	2°	2°
Pathloss exponent	3	3
Number of subcarriers (K)	16	32
Cyclic prefix length	$K/4$	$K/4$
Number RF chains	2	2
Number spatial streams	2	2
Angle between FD arrays	$\pi/2$	$\pi/2$
Distance between FD arrays	2λ	2λ
Signal-to-Interference Ratio	-120 dB	-120 dB
Rician factor	5 dB	5 dB
Raised cosine roll-off factor	1	1
Outer iterations (N_{outer})	10	10

A. Primary Evaluation

Fig. 4 presents spectral efficiency results vs. average SNR. Primarily, we observe the full-digital design simulated with $N_{\text{outer}} = 10$ iterations is robust to the SI and very close to the upper bound. Unlike the full-digital case, the hybrid beamforming design experiences limitations observed mainly for the uplink, even though the downlink scheme seems to be very close to the full-digital performance since the downlink UE is interference-free. In the downlink, the small gap between the full-digital and hybrid beamforming is caused by the losses incurred by the hardware constraint. In addition, we observe that uplink performance improves with the number of inner alternating projections. The low performance at $N_{\text{inner}} = 10$ iterations is due to the zero-forcing constraint being approximately but not completely satisfied; hence, the

³For all cases, 1000 realizations of the random variables were generated to perform the Monte Carlo simulation in MATLAB.

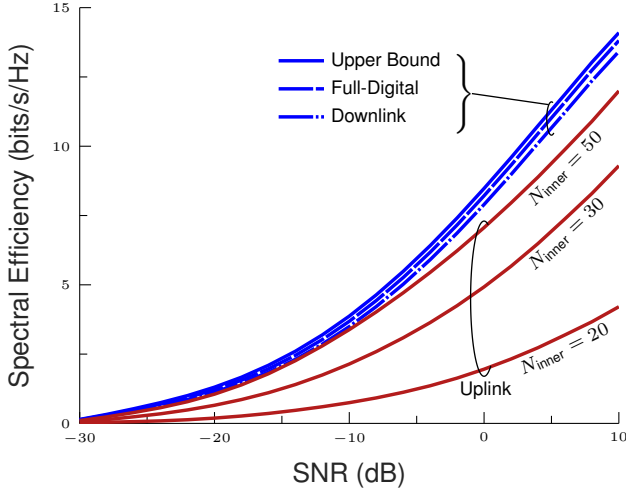


Fig. 4: Spectral efficiency results: Performance is evaluated in terms of uplink and downlink spectral efficiency for hybrid architecture. The uplink rate is evaluated for different number of iterations of the inner loop corresponding to alternating projections. In addition, full-digital and upper bound are evaluated and serve as benchmarking tools. MmWave configuration is considered for this simulation.

optimal precoders and combiners are not yet obtained. At $N_{\text{inner}} = 50$ iterations, the beamformers are closely projected onto the zero-forcing null-space, which further enhances the uplink rate. The results are confirmed by [32] but for machine-to-machine narrowband FD systems.

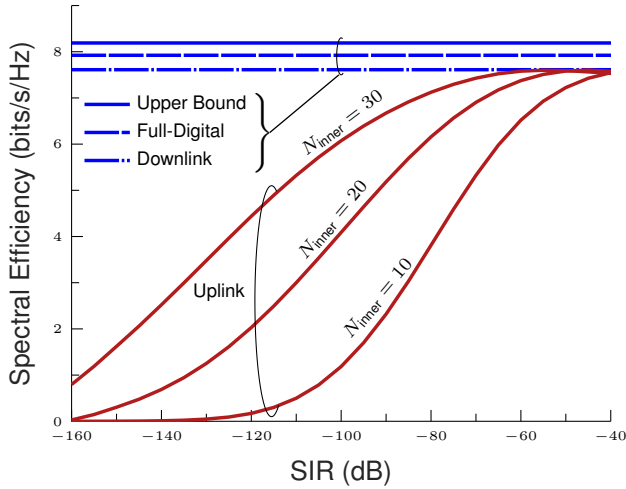


Fig. 5: Spectral efficiency results: Performances are evaluated at SNR = 0 dB and across a range of SIR from -160 to -40 dB which corresponds to cell-edge user (-160 dB), middle user (around -80 dB) and near user (-40 dB), respectively. The algorithm robustness is tested for various number of iterations of the alternating projections routine. Note that mmWave setting is assumed for this scenario.

B. Alternating Projections and Signal-to-Interference Ratio

Fig. 5 presents the spectral efficiency for different numbers of inner loop alternating projections across a range of SIRs. The full-digital beamformer remains close to the upper bound while the downlink rate for hybrid architecture is still limited by the hardware constraint. In accordance with the conclusions drawn from Fig. 4, the uplink rate improves with the number of inner loop alternating projections. We further observe that

the design is sensitive to high SI power (SIR between -160 and -140 dB) specifically for a few inner iterations. However, the performance can be further improved by running more iterations of alternating projections. As SIR increases to around -40 dB which corresponds to a user near the BS, the uplink performance matches the downlink (interference-free) performance regardless of the number of iterations.

C. Proposed vs. Conventional Approaches

Fig. 6 compares proposed and conventional approaches implemented in analog-only architectures. We observe that conventional designs are very sensitive to the SI because the zero-forcing and hardware conditions are not properly handled. In contrast, the proposed design is more resilient to SI and achieves higher sum spectral efficiency around 13 bits/s/Hz at 10 dB of SNR whereas beam steering, SVD and angle search techniques achieve roughly 9, 9, and 7 bits/s/Hz.

D. Degrees of Freedom

Fig. 7 illustrates the outage performance with respect to a given range of target rate requirements for 16 and 64 antennas at the relay/BS, respectively. We observe that for the same inner alternating projections iterations, the gap between the uplink and downlink rate for hybrid architectures changes with the number of antennas. As we conclude so far, the rate performances improve with the number of iterations of alternating projections, however, this improvement is also limited by the number of antennas. In fact, the number of antennas are shared between providing spatial multiplexing gain (sustain enough number of spatial streams) and SI cancellation. If the number of antennas is low, then there is not enough degree of freedom to perfectly eliminate the SI and hence the alternating projections routine (length of iterations) becomes useless, i.e., increasing N_{inner} does not bring any further enhancement. The 64 antennas setting which provides enough degree of freedom

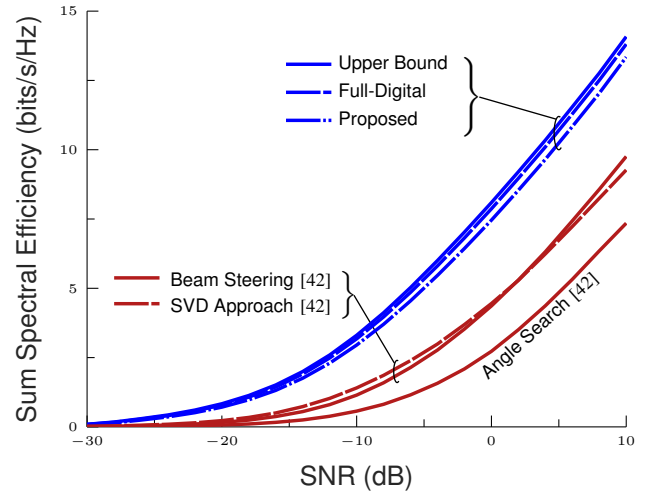


Fig. 6: Sum spectral efficiency results: Comparisons are made between the proposed and conventional approaches. Note that the conventional techniques presented in [42] are developed for machine to machine FD systems. In this work, we changed these techniques accordingly to support the proposed system model. These performances are evaluated for analog-only architecture in accordance with [42]. We adopt the sub-6 GHz setting for this scenario.

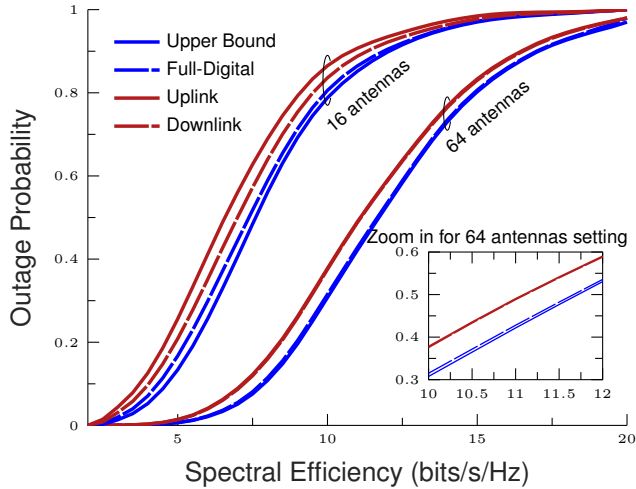


Fig. 7: Outage probability results: Comparisons are made between uplink and downlink scenarios for hybrid beamforming with full-digital as well as upper bound which serve as benchmarking tools. In addition, the comparison involves two settings with 16 and 64 antennas at the BS/relay. MmWave configuration is considered in this scenario while the SNR is maintained at 0 dB while $N_{\text{inner}} = 50$ iterations.

provides not only the spectral efficiency (multiplexing gain) but also perfectly cancel the SI which is observed by the complete matching between the uplink and downlink rates.

E. Power Consumption and RF Chains

In this simulation, we will evaluate the energy efficiency for different variants wherein the relative parameters of each one is provided by Table III.

Fig. 8 illustrates the energy efficiency as a function of the number of RF chains at the relay/BS for different variants. We observe that for low number of RF chain, variant 1 seems to be well advocated for power-efficient systems as it provides better energy efficiency compared to the other variants. This is explained by the fact that for a few number of RF chains, the rate at which the power consumption increases is higher than the rate of spectral efficiency. However, as the number of RF chains increases, the spectral efficiency improves at higher rate compared to the power consumption as a function of the RF chains wherein variant 4 becomes the best one since it provides hefty beamforming gain from the massive number of antennas. Furthermore, the effect of the ADC power can be easily observed by comparing variants 2 and 3 (having the same number of antennas). We notice that variant 2 is more power-efficient than variant 3 since the latter requires more ADC power. We also note that variant 2 remains more power-efficient than variant 3 across all the number of RF chains.

TABLE III
PARAMETERS OF EACH VARIANT [1], [43].

Parameter	Variant 1	Variant 2	Variant 3	Variant 4
Frequency	28 GHz	39 GHz	39 GHz	73 GHz
Bandwidth	850 MHz	1.4 GHz	1.6 GHz	2 GHz
ADC Power	250 mW	400 mW	450 mW	550 mW
BS Antennas	32	64	64	128

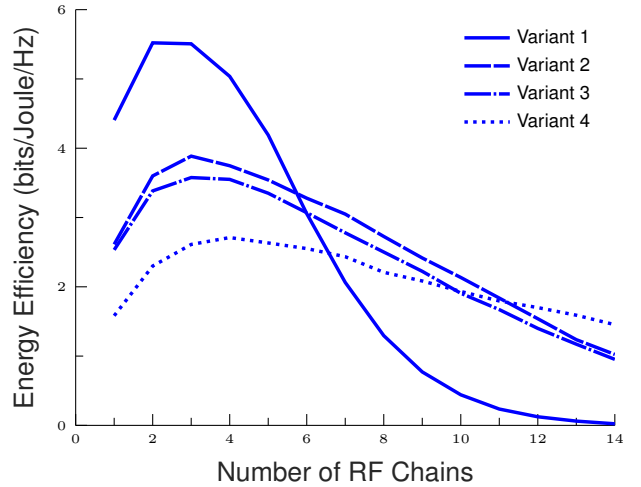


Fig. 8: Energy efficiency performance: Results are evaluated for four variants and for different number of RF chains at the relay/BS. The SNR is fixed at 0 dB. The simulations are performed for uplink scenario with $N_{\text{inner}} = 50$ iterations.

VI. CONCLUSION

For mmWave communications using hybrid analog/digital beamformers, we analyzed a single-cell, single-user MIMO scenario in which the uplink and downlink UEs are simultaneously communicating with a full-duplex relay/BS. We proposed algorithms to design the hybrid beamformers that are already built into FD relay to maximize the uplink plus downlink sum capacity while bringing the SI below the noise floor. Our approach uses the hybrid beamformers already built into the 5G mmWave system, and hence, does not need any additional circuitry. We showed that the spectral efficiency improves with the number of inner alternating projection iterations and that the overall the enhancement is limited by the available degrees of freedom. We concluded that the proposed technique is more efficient in SI cancellation than conventional beamsteering, SVD and angle search techniques.

Although spectral efficiency and outage probability remain important measures, energy efficiency is also an important concern due to the high power consumption for transceiver architectures to support mmWave bands. We evaluated energy efficiency for 28, 39 and 73 GHz mmWave band variants and showed how the behavior depends on the number of RF chains. We also noticed that ADC power consumption can significantly impact energy efficiency, as illustrated by variants in the 39 GHz band.

An important future direction is the joint optimization of spectral and energy efficiency in designing the beamformers with low resolution ADCs.

REFERENCES

- [1] R. W. Heath, N. González-Prelcic, S. Rangan, W. Roh, and A. M. Sayeed, "An overview of signal processing techniques for millimeter wave MIMO systems," *IEEE Journal of Selected Topics in Signal Processing*, vol. 10, no. 3, pp. 436–453, 2016.
- [2] E. Onggosanusi, M. S. Rahman, L. Guo, Y. Kwak, H. Noh, Y. Kim, S. Faxer, M. Harrison, M. Frenne, S. Grant, R. Chen, R. Tamrakar, and a. Q. Gao, "Modular and high-resolution channel state information and beam management for 5G new radio," *IEEE Communications Magazine*, vol. 56, no. 3, pp. 48–55, 2018.

- [3] E. Balti and B. K. Johnson, "Tractable approach to mmwaves cellular analysis with FSO backhauling under feedback delay and hardware limitations," *IEEE Transactions on Wireless Communications*, vol. 19, no. 1, pp. 410–422, 2020.
- [4] R. Askar, J. Chung, Z. Guo, H. Ko, W. Keusgen, and T. Haustein, "Interference handling challenges toward full duplex evolution in 5G and beyond cellular networks," *IEEE Wireless Communications*, vol. 28, no. 1, pp. 51–59, Feb. 2021.
- [5] A. Sahai, G. Patel, and A. Sabharwal, "Pushing the limits of full-duplex: Design and real-time implementation," *CoRR*, vol. abs/1107.0607, 2011. [Online]. Available: <http://arxiv.org/abs/1107.0607>
- [6] A. Sahai, G. Patel, and A. Sabharwal, "Asynchronous full-duplex wireless," in *International Conference on Communication Systems and Networks*, Jan 2012, pp. 1–9.
- [7] C. R. Anderson, S. Krishnamoorthy, C. G. Ranson, T. J. Lemon, W. G. Newhall, T. Kummert, and J. H. Reed, "Antenna isolation, wideband multipath propagation measurements, and interference mitigation for on-frequency repeaters," in *IEEE SoutheastCon*, March 2004, pp. 110–114.
- [8] K. Haneda, E. Kahra, S. Wyne, C. Icheln, and P. Vainikainen, "Measurement of loop-back interference channels for outdoor-to-indoor full-duplex radio relays," in *European Conference on Antennas and Propagation*, April 2010, pp. 1–5.
- [9] M. Jain, J. I. Choi, T. Kim, D. Bharadia, S. Seth, K. Srinivasan, P. Levis, S. Katti, and P. Sinha, "Practical, real-time, full duplex wireless," in *ACM International Conference on Mobile Computing and Networking*, 2011, p. 301–312. [Online]. Available: <https://doi.org/10.1145/2030613.2030647>
- [10] E. Everett, M. Duarte, C. Dick, and A. Sabharwal, "Empowering full-duplex wireless communication by exploiting directional diversity," in *Asilomar Conference on Signals, Systems and Computers*, Nov 2011, pp. 2002–2006.
- [11] E. Everett, A. Sahai, and A. Sabharwal, "Passive self-interference suppression for full-duplex infrastructure nodes," *IEEE Transactions on Wireless Communications*, vol. 13, no. 2, pp. 680–694, Feb. 2014.
- [12] M. A. Khojastepour, K. Sundaresan, S. Rangarajan, X. Zhang, and S. Barghi, "The case for antenna cancellation for scalable full-duplex wireless communications," in *ACM Workshop on Hot Topics in Networks*, 2011. [Online]. Available: <https://doi.org/10.1145/2070562.2070579>
- [13] J. I. Choi, S. Hong, M. Jain, S. Katti, P. Levis, and J. Mehlman, "Beyond full duplex wireless," in *Asilomar Conference on Signals, Systems and Computers*, Nov. 2012, pp. 40–44.
- [14] M. Duarte, A. Sabharwal, V. Aggarwal, R. Jana, K. K. Ramakrishnan, C. W. Rice, and N. K. Shankaranarayanan, "Design and characterization of a full-duplex multi-antenna system for wifi networks," *IEEE Transactions on Vehicular Technology*, vol. 63, no. 3, pp. 1160–1177, Mar. 2014.
- [15] M. Duarte, C. Dick, and A. Sabharwal, "Experiment-driven characterization of full-duplex wireless systems," *IEEE Transactions on Wireless Communications*, vol. 11, no. 12, pp. 4296–4307, Dec. 2012.
- [16] J. I. Choi, M. Jain, K. Srinivasan, P. Levis, and S. Katti, "Achieving single channel, full duplex wireless communication," in *ACM International Conference on Mobile Computing and Networking*, 2010, p. 1–12. [Online]. Available: <https://doi.org/10.1145/1859995.1859997>
- [17] Q. Wang, Y. Dong, X. Xu, and X. Tao, "Outage probability of full-duplex af relaying with processing delay and residual self-interference," *IEEE Communications Letters*, vol. 19, no. 5, pp. 783–786, May 2015.
- [18] E. Balti and M. Guizani, "Impact of non-linear high-power amplifiers on cooperative relaying systems," *IEEE Transactions on Communications*, vol. 65, no. 10, pp. 4163–4175, 2017.
- [19] B. P. Day, A. R. Margetts, D. W. Bliss, and P. Schniter, "Full-duplex bidirectional mimo: Achievable rates under limited dynamic range," *IEEE Transactions on Signal Processing*, vol. 60, no. 7, pp. 3702–3713, Jul. 2012.
- [20] E. Everett, C. Shepard, L. Zhong, and A. Sabharwal, "SoftNull: Many-antenna full-duplex wireless via digital beamforming," *IEEE Transactions on Wireless Communications*, vol. 15, no. 12, pp. 8077–8092, Dec. 2016.
- [21] Z. Xiao, P. Xia, and X. Xia, "Full-duplex millimeter-wave communication," *IEEE Wireless Communications*, vol. 24, no. 6, pp. 136–143, Dec. 2017.
- [22] K. Satyanarayana, M. El-Hajjar, P. Kuo, A. Mourad, and L. Hanzo, "Hybrid beamforming design for full-duplex millimeter wave communication," *IEEE Transactions on Vehicular Technology*, vol. 68, no. 2, pp. 1394–1404, 2019.
- [23] H. Abbas and K. Hamdi, "Full duplex relay in millimeter wave backhaul links," in *IEEE Wireless Communications and Networking Conference*, 2016, pp. 1–6.
- [24] A. Ali, N. González-Prelcic, and R. W. Heath, "Millimeter wave beam-selection using out-of-band spatial information," *IEEE Transactions on Wireless Communications*, vol. 17, no. 2, pp. 1038–1052, 2018.
- [25] I. P. Roberts, H. B. Jain, and S. Vishwanath, "Frequency-selective beamforming cancellation design for millimeter-wave full-duplex," in *IEEE International Conference on Communications*, 2020, pp. 1–6.
- [26] E. Balti and N. Mensi, "Zero-forcing max-power beamforming for hybrid mmWave full-duplex MIMO systems," in *IEEE International Conference on Advanced Systems and Emergent Technologies*, 2020.
- [27] E. Balti, M. Guizani, B. Hamdaoui, and B. Khalfi, "Aggregate hardware impairments over mixed RF/FSO relaying systems with outdated CSI," *IEEE Transactions on Communications*, vol. 66, no. 3, pp. 1110–1123, 2018.
- [28] Y. Maalej, A. Abderrahim, M. Guizani, B. Hamdaoui, and E. Balti, "Advanced activity-aware multi-channel operations in vanets for vehicular clouds," in *IEEE Global Communications Conference*, 2016, pp. 1–6.
- [29] D. Korpi, T. Riihonen, V. Syrjäälä, L. Anttila, M. Valkama, and R. Wichman, "Full-duplex transceiver system calculations: Analysis of ADC and linearity challenges," *IEEE Transactions on Wireless Communications*, vol. 13, pp. 3821–3836, 2014.
- [30] D. Kim, H. Ju, S. Park, and D. Hong, "Effects of channel estimation error on full-duplex two-way networks," *IEEE Transactions on Vehicular Technology*, vol. 62, pp. 4666–4672, 2013.
- [31] A. Sahai, G. Patel, C. Dick, and A. Sabharwal, "On the impact of phase noise on active cancellation in wireless full-duplex," *IEEE Transactions on Vehicular Technology*, vol. 62, pp. 4494–4510, 2013.
- [32] R. López-Valcarce and M. Martínez-Cotelo, "Full-duplex mmWave communication with hybrid precoding and combining," in *European Signal Processing Conference*, Amsterdam (Netherlands), 08/2020 2020.
- [33] Z. Xiao, P. Xia, and X. Xia, "Full-duplex millimeter-wave communication," *IEEE Wireless Communications*, vol. 24, no. 6, pp. 136–143, 2017.
- [34] M. R. René Escalante, *Alternating Projection Methods*, ser. Fundamentals of Algorithms. SIAM, 2011.
- [35] R. López-Valcarce and N. González-Prelcic, "Analog beamforming for full-duplex millimeter wave communication," in *International Symposium on Wireless Communication Systems*, 2019, pp. 687–691.
- [36] W. B. Abbas, F. Gomez-Cuba, and M. Zorzi, "Millimeter wave receiver efficiency: A comprehensive comparison of beamforming schemes with low resolution adcs," *IEEE Transactions on Wireless Communications*, vol. 16, no. 12, pp. 8131–8146, 2017.
- [37] Y. Yu, P. G. M. Baltus, A. de Grauw, E. van der Heijden, C. S. Vaucher, and A. H. M. van Roermund, "A 60 ghz phase shifter integrated with LNA and PA in 65nm CMOS for phased array systems," *IEEE Journal of Solid-State Circuits*, vol. 45, no. 9, pp. 1697–1709, 2010.
- [38] L. Kong, "Energy-efficient 60GHz phased-array design for Multi-Gb/s communication systems," Ph.D. dissertation, EECS Department, University of California, Berkeley, Dec 2014. [Online]. Available: <http://www2.eecs.berkeley.edu/Pubs/TechRpts/2014/EECS-2014-191.html>
- [39] Yu-Hsuan Lin and H. Wang, "A low phase and gain error passive phase shifter in 90nm CMOS for 60GHz phase array system application," in *IEEE MTT-S International Microwave Symposium*, 2016, pp. 1–4.
- [40] M. Kraemer, D. Dragomirescu, and R. Plana, "Design of a very low-power, low-cost 60GHz receiver front-end implemented in 65nm CMOS technology," *International Journal of Microwave and Wireless Technologies*, vol. 3, no. 2, p. 131–138, 2011.
- [41] R. Méndez-Rial, C. Rusu, N. González-Prelcic, A. Alkhateeb, and R. W. Heath, "Hybrid mimo architectures for millimeter wave communications: Phase shifters or switches?" *IEEE Access*, vol. 4, pp. 247–267, 2016.
- [42] X. Liu, Z. Xiao, L. Bai, J. Choi, P. Xia, and X.-G. Xia, "Beamforming Based Full-Duplex for Millimeter-Wave Communication," *Sensors*, vol. 16, no. 7, 2016.
- [43] "mmWave: The Battle of the Bands." [Online]. Available: <https://www.ni.com/en-us/innovations/white-papers/16/mmwave--the-battle-of-the-bands.html>